Electrocatalytic metal hydride generation using CPET mediators

https://doi.org/10.1038/s41586-022-04874-z

Received: 15 July 2021

Accepted: 16 May 2022

Subal Dey[1,2], **Fabio Masero**[1], **Enzo Brack**[1], **Marc Fontecave**[2] & **Victor Mougel**[1]✉

Transition metal hydrides (M-H) are ubiquitous intermediates in a wide range of enzymatic processes and catalytic reactions, playing a central role in H^+/H_2 interconversion[1], the reduction of CO_2 to formic acid (HCOOH)[2] and in hydrogenation reactions. The facile formation of M-H is a critical challenge to address to further improve the energy efficiency of these reactions. Specifically, the easy electrochemical generation of M-H using mild proton sources is key to enable high selectivity versus competitive CO and H_2 formation in the CO_2 electroreduction to HCOOH, the highest value-added CO_2 reduction product[3]. Here we introduce a strategy for electrocatalytic M-H generation using concerted proton–electron transfer (CPET) mediators. As a proof of principle, the combination of a series of CPET mediators with the CO_2 electroreduction catalyst $[Mn^I(bpy)(CO)_3Br]$ (bpy = 2,2′-bipyridine) was investigated, probing the reversal of the product selectivity from CO to HCOOH to evaluate the efficiency of the manganese hydride (Mn-H) generation step. We demonstrate the formation of the Mn-H species by in situ spectroscopic techniques and determine the thermodynamic boundary conditions for this mechanism to occur. A synthetic iron–sulfur cluster is identified as the best CPET mediator for the system, enabling the preparation of a benchmark catalytic system for HCOOH generation.

In mechanistic terms, the electrochemical generation of transition metal hydrides (M-H) typically requires the reduction of the metal centre, followed by the transfer of a proton and an electron in a stepwise fashion, via an electron transfer–proton transfer (ET–PT), or PT–ET, sequence (Fig. 1a, grey box)[4,5]. Such sequential processes involve the transfer of electrons and protons from different sources (the electrode and the electrolyte, respectively). Whereas mildly reactive M-H (that is, displaying high hydricity and bond dissociation free energy (BDFE) values) may be generated at modest potentials using mild acid sources[4,6], the most reactive M-H—of interest in the context of CO_2 reduction—require generation of highly reduced metal centres or the use of strong acids, which lowers the energy efficiency and rates. Major advances in M-H-mediated electrocatalysis have resulted from improving the ET step with redox mediators[7,8] or the PT step using proton shuttles[1,9,10].

We propose here an alternative strategy for the electrochemical generation of M-H, involving the overall transfer of an electrogenerated hydrogen atom (that is, an electron and a proton) to the metal centre in one kinetic step, called concerted proton–electron transfer (CPET) (Fig. 1a, blue box). This enables higher rates while requiring only low driving forces, that is, moderate reducing potentials and weak acids. The use of milder proton sources thus minimizes the chances of quenching the hydride species to generate H_2, a main point to enable high selectivity when H_2 is not the targeted product. Such a concerted process necessitates a mediator that is able to collect an electron from the electrode and a proton from the electrolyte, and to transfer them concertedly as an overall hydrogen atom to generate the M-H species. A few examples of such CPET mediators have been shown to be very successful at increasing reaction rates in both oxidative[11–13] and reductive processes[14,15]. However, to the best of our knowledge, the use of a CPET mediator to mediate the electrocatalytic generation of a metal hydride has not been reported.

Herein, we demonstrate that the use of appropriately chosen CPET mediators enables the energy-efficient electrocatalytic generation of M-H species, and we explore the potential of this approach for the electrocatalytic transformation of CO_2 (Fig. 1b). We report that the iron–sulfur cluster $[Fe_4S_4(SPh)_4]^{2-}$ (**Fe-S**) can be used as a CPET mediator in the presence of $[Mn^I(bpy)(CO)_3Br]$ (**Mn^I-cat**) to promote the electrocatalytic formation of Mn-H species. We demonstrate that this strategy enables shifting of the CO_2 reduction reaction (CO_2RR) selectivity of **Mn^I-cat** from CO to HCOOH, identifying one of the most active catalytic systems for the selective reduction of CO_2 to HCOOH. This example enabled us to validate the boundary conditions for the choice of CPET mediators applicable in the electrochemical generation of metal hydrides.

CPET-mediated M-H formation applied to CO_2RR

The choice of an appropriate CPET mediator (med) for catalytic M-H formation requires optimizing two CPET steps: (1) the (re)generation of the med-H species with an electron and a proton; and (2) the overall transfer of an apparent hydrogen atom (that is, a proton and an

---

[1]Department of Chemistry and Applied Biosciences, ETH Zürich, Zurich, Switzerland. [2]Laboratoire de Chimie des Processus Biologiques, UMR 8229 CNRS, Collège de France, Sorbonne Université, Paris, France. ✉e-mail: mougel@inorg.chem.ethz.ch

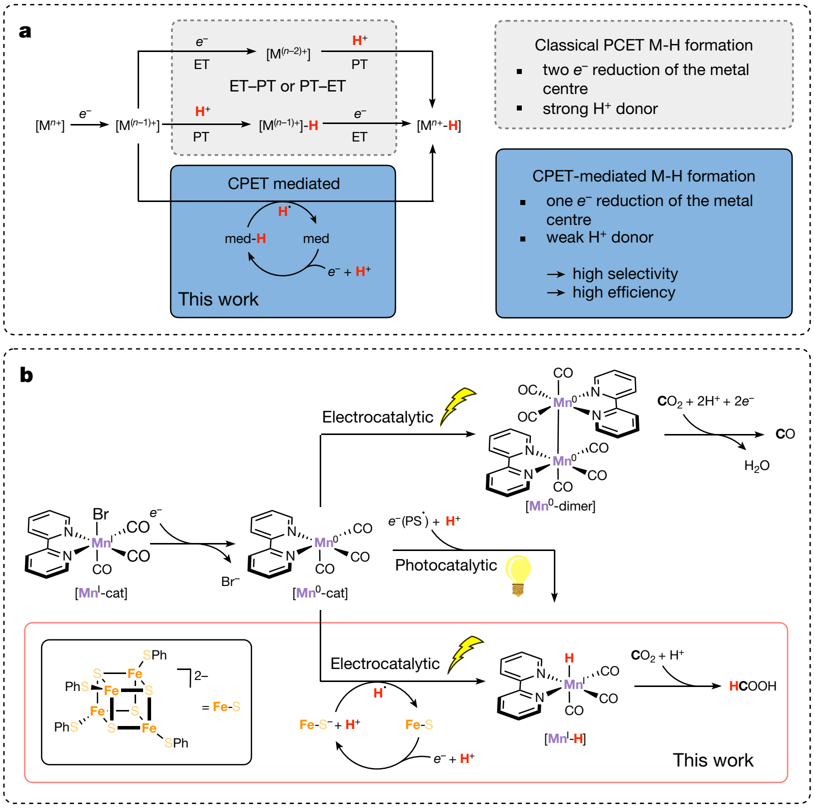

Fig. 1 | CPET-mediated metal hydride formation. a, Generation of M-H species via stepwise proton-coupled electron transfer (PCET: ET–PT or PT–ET, grey box) and CPET (blue box) processes. The superscripts indicate metal oxidation states. **b**, Reaction pathways and associated product selectivity for **Mn$^{\text{I}}$-cat**-catalysed CO$_2$ reduction under electro- and photochemical conditions.

electron) to the singly reduced metal site (Fig. 1a, blue box). The thermodynamic and kinetic parameters required for efficient M-H generation using a CPET mediator are ultimately fixed by the BDFE and pK_a values of the generated hydride species. Thus, the choice of the CPET mediator used should be tailored to the M-H species targeted and ultimately to the desired catalytic application. In the present work, we investigated the impact of the proposed CPET-mediated generation of M-H in the context of CO$_2$ electroreduction, as the formation of M-H intermediates is known to affect the catalyst's selectivity and product distribution. The vast majority of molecular electrocatalysts for CO$_2$RR promote two-electron reduction of CO$_2$ to CO or HCOOH, the latter generally requiring formation of an M-H intermediate, whereas CO formation typically requires the direct interaction of CO$_2$ with the metal centre and precludes M-H formation[2]. Among the widely investigated selective CO$_2$RR catalysts, we selected **Mn$^{\text{I}}$-cat**, given its divergent behaviour in electrochemical and photochemical CO$_2$RR (Fig. 1b). It produces CO under electrochemical conditions[16], whereas HCOOH is generated as the major product under photochemical conditions[17]. This change of selectivity relates directly to the reaction pathway involved during catalysis: the C-centred activation of CO$_2$ under electrochemical conditions leads to CO as the main product, whereas the Mn-H species formed under photochemical conditions enables HCOOH formation[18]. The factors influencing the formation of Mn-H species in such molecular complexes under photochemical conditions are, however, not fully understood. Related to this, recent studies highlighted that the proximity of proton donors in the ligand framework may enable the generation of Mn-H species also under electrochemical conditions[19,20].

An initial screening of the thermodynamic feasibility of such a CPET-mediated Mn-H formation using reported BDFE values[21,22] (see below) motivated our choice of iron–sulfur clusters (Fe–S clusters) as CPET mediators. Synthetic Fe–S clusters have so far not been exploited to mediate CPET steps in a catalytic context. However, proton-coupled electron transfer-mediated by Fe–S clusters have been observed in Fe–Fe hydrogenases[23] (H cluster) as well as in 3Fe–4S cluster-containing ferredoxins[24], and recent studies have shown that synthetic Fe–S clusters are also capable of donating or accepting an effective H atom in a stoichiometric reaction[21,25]. In addition, their very low reorganization energy, which is key to the high efficiency of electron transfers in enzymatic systems[26,27], is highly desirable for efficient (re)generation when used as a CPET mediator. Last, the multiple site nature of CPET on Fe–S clusters, in which protonation occurs at a sulfur base, whereas reduction occurs at a Fe centre, may constitute a kinetic advantage over the use of a metal hydride to carry out the same function as the CPET mediator, because the kinetics of metal hydride formation may be hampered by higher reorganization energy costs[6,28]. On the basis of these facts, we investigated the CO$_2$RR using the synthetic iron–sulfur cluster, **Fe-S**, as a potential CPET mediator, in combination with the well-known CO$_2$ reduction catalyst **Mn$^{\text{I}}$-cat**.

Under an argon atmosphere, the cyclic voltammogram (CV) of a 1:1 mixture of both **Mn$^{\text{I}}$-cat** and **Fe-S** cluster in acetonitrile (CH$_3$CN) is seen to be identical to the sum of the CVs of its individual components, revealing three consecutive 1e^- reduction events at −1.34 V, −1.65 V and −1.89 V (Supplementary Fig. 1; potentials expressed versus Fc/Fc$^+$ (ferrocene/ferrocenium) here and in all text below). These events were assigned, respectively, to the **Fe-S**$^{0/-1}$ redox process, to the reduction of **Mn$^{\text{I}}$-cat** to the dimeric complex [Mn^0(bpy)(CO)$_3$]$_2$ (**Mn^0-dimer**) and the subsequent reduction of the dimer to the **Mn^{-1}-cat** species (Fig. 1b and Supplementary Section 2.1.1).

This behaviour is markedly different under CO$_2$RR conditions using 2,2,2-trifluoroethanol (TFE) as the proton source (Supplementary

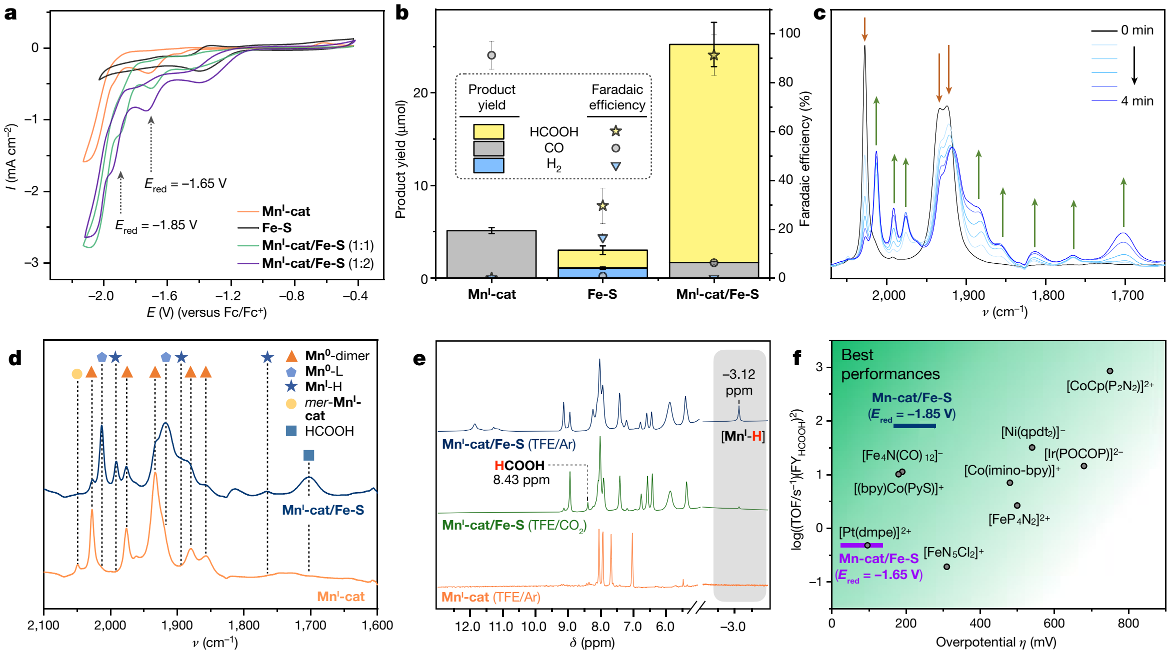

Fig. 2 | Catalytic activity and spectroscopic characterization of relevant intermediates of CPET-mediated CO_2RR activity of Mn^I-cat. a, Overlaid CV traces of **Mn^I-cat** (1 mM) in the absence and in the presence of **Fe-S** along with the CV of **Fe-S** alone (0.2 M TFE, 0.1 M $TBAPF_6$ in CH_3CN). **b**, Corresponding products, and associated FY obtained during 90 min CPE at −1.85 V using a 1:2 **Mn^I-cat/Fe-S** mixture (0.2 M TFE, 0.1 M $TBAPF_6$ in CO_2-saturated CH_3CN). Thick lines error bars indicate the systematic error of duplicate CPE measurements and thin line error bars correspond to the standard deviation of three independent GC injections. **c**, Time-dependent evolution of IRSEC signals of a 1:2 **Mn^I-cat/Fe-S** mixture in the presence of CO_2 on reduction at −1.65 V (40 equiv. TFE, 0.1 M $TBAPF_6$ in CO_2-saturated CH_3CN). **d**, Overlay of IRSEC signals after 4 min CPE of a 1:2 **Mn^I-cat/Fe-S** mixture (blue) and **Mn^I-cat** only (orange) under the conditions described in **c**. **e**, Ex situ ^1H NMR spectra recorded after CPE of **Mn^I-cat** (orange) and a 1:1 **Mn^I-cat/Fe-S** mixture at −1.65 V and addition of TFE (50 equiv.) under Ar (blue) and CO_2 (green). **f**, Comparison of the performance among reported catalytic CO_2RR systems selective for HCOOH production (Supplementary Section 2.8 and Supplementary Table 3). The bars indicate the range of overpotential for the **Mn^I-cat/Fe-S** system. To account for the uncertainties related to the actual pK_a value of the proton source in solution: the formation of HCOOH under catalytic conditions used here was experimentally confirmed via FTIR studies, but cannot be rationalized using the pK_a values reported for TFE (25.1) and determined here for HCOOH (21.6) (Supplementary Sections 2.3 and 2.5).

Section 2.1.1 and Supplementary Figs. 1–6). The CV of the 1:1 mixture of **Mn^I-cat** and **Fe-S** presented in Fig. 2a exhibits two significant changes with respect to the CVs of each complex taken separately: the catalytic current of the peak assigned to the electrochemical CO_2RR activity of **Mn^I-cat** at −2.05 V is enhanced by approximately 50%, and a new catalytic feature appears at −1.85 V (note that **Fe-S** alone does not show any catalytic features within the experimental potential range). In addition, a small current enhancement (2.4 times) of the peak at −1.65 V is observed under CO_2RR conditions. In the absence of CO_2 or TFE, the catalytic process at −2.05 V is not present and the process at −1.85 V is substantially lowered, whereas the **Fe-S$^{0/-1}$** process remained unaltered (Supplementary Figs. 2 and 3). Increasing the concentration of **Fe-S** (1:2 **Mn^I-cat/Fe-S** ratio) does not affect the current of the −2.05 V peak, but results in a further increase of the catalytic current at −1.85 V (Fig. 2a). These results suggest that the new catalytic process at −1.85 V is related to the generation of a new catalytic species resulting from the synergistic combination of **Fe-S** and **Mn^I-cat** and occurring at less negative potentials than that required for **Mn^I-cat** alone to reduce CO_2. To identify the reaction catalysed at this new catalytic process, we carried out a series of 90 min controlled potential electrolyses (CPEs) (Supplementary Fig. 7). A CPE at −1.85 V revealed a complete shift of product selectivity and formation rates (Fig. 2b): the combination of **Mn^I-cat** and **Fe-S** (1:2 ratio) enabled the formation of a large amount of HCOOH with high selectivity (Faradaic yield (FY_{HCOOH}) = 92%, product yield (n_{HCOOH}) = 23 μmol) and a small amount of CO (FY_{CO} = 6%, n_{CO} = 1.6 μmol), whereas **Mn^I-cat** alone catalyses CO_2RR selectively, as expected, to CO with low activity (FY_{CO} = 91%, n_{CO} = 5 μmol) with no formation of H_2, and **Fe-S** alone only produces a very small amount of HCOOH (FY_{HCOOH} = 30%, n_{HCOOH} = 1.9 μmol) and H_2 (FY_{H_2} = 17%, n_{H_2} = 1 μmol) (Supplementary Table 1). We identified the 1:2 **Mn^I-cat/Fe-S** ratio as optimal, as both the amount of products formed and the selectivity for HCOOH versus CO were enhanced when increasing the concentration of **Fe-S** (that is, decreasing the **Mn^I-cat/Fe-S** ratio), reaching a plateau at a 1:2 ratio (Supplementary Fig. 7 and Supplementary Table 1). With an overall turnover frequency (TOF) of 20 s^{-1} at an overpotential of only 22–340 mV (Fig. 2 and Supplementary Section 2.5) measured from the long-term CPE experiment, the 1:2 **Mn^I-cat/Fe-S** system stands among the best molecular electrocatalytic systems for the reduction of CO_2 to HCOOH, while operating at remarkably high Faradaic efficiency (Fig. 2f and Supplementary Section 2.8). In addition, independently of the selectivity shift, an approximately fivefold increase in turnover number (TON) for CO_2RR was observed with respect to the analogous CPE carried out in the absence of **Fe-S** (Supplementary Table 1).

Finally, the origin of the above-mentioned increase of the current at −1.65 V under catalytic conditions with the 1:2 **Mn^I-cat/Fe-S** system was investigated by carrying out a CPE at −1.65 V. Selective HCOOH formation was also observed (FY_{HCOOH} = 78%, n_{HCOOH} = 7.6 μmol; Supplementary Table 1) yet with significantly lower rates (TOF = 0.4 s^{-1}) than at −1.85 V. Nevertheless, selective reduction of CO_2 to HCOOH at such a modest overpotential (20–140 mV) is, to our knowledge, unprecedented for first-row transition metal catalysts (Fig. 2f). In addition, we suspect parasitic side reactions, significant at such low currents, to account for the remaining FY, as significantly increased FY for HCOOH were observed at −1.7 V (FY_{HCOOH} = 91%, n_{HCOOH} = 9.5 μmol;

Supplementary Table 1). Last, CPE at the third catalytic wave (E_{red} = −2.05 V) with a 1:2 ratio of **Mn^{I}-Cat/Fe-S** revealed an increased CO:HCOOH ratio (FY_{CO} = 32%, FY_{HCOOH} = 56%) together with small amounts of H_2 (FY_{H_2} = 6%). This lowered selectivity for HCOOH is consistent with the combination of the catalytic process at −1.85 V, mentioned above, and the catalytic process at −2.05 V originating from the residual activity of **Mn^{I}-Cat**, as suggested by the CV studies. Decomposition of the complexes under catalytic conditions and modulation of the reactivity by potential side products of the solvolysis of **Fe-S** were ruled out (Supplementary Section 2.9 and Supplementary Figs. 11 and 12).

Spectroscopic identification of Mn-H species

Such a change of selectivity from CO to HCOOH suggests the formation of a Mn-H intermediate[19,20] in the presence of **Fe-S** and prompted us to investigate reaction intermediates via in situ spectroscopic techniques. Infrared spectro-electrochemical (IRSEC) studies under optimized catalytic conditions (CO_2-saturated electrolyte solution, 40 equiv. TFE, 2 mM **Mn^{I}-cat** and 4 mM **Fe-S**), revealed the appearance of the characteristic ν_{CO} vibrations of the Mn(I) hydride complex [$Mn^{I}(bpy)(CO)_3H$] (**Mn^{I}-H**) at 1,990 and 1,892 cm^{-1}, together with a weak vibration at 1,764 cm^{-1}, when the potential of the cell was held below −1.65 V (Fig. 2c). Whereas the carbonyl stretches ν_{CO} of **Mn^{I}-H** have been reported[19,29], the new band at 1,764 cm^{-1} observed here can be tentatively assigned to the corresponding $\nu_{Mn\text{-}H}$ stretch of **Mn^{I}-H**, as it lies in the range of reported Mn^{I}-H vibrations[30] and was not present when using deuterated TFE (TFED) instead of TFE (Supplementary Fig. 16). None of the vibrations associated with **Mn^{I}-H** were observed in the absence of **Fe-S** or TFE (Supplementary Fig. 14). With respect to the IRSEC spectrum recorded in the absence of **Fe-S** (Fig. 2d, orange trace), a striking feature of the 1:2 **Mn^{I}-cat/Fe-S** spectrum (Fig. 2d, blue trace) is the relatively lower intensity of the ν_{CO} vibrations at 1,975, 1,934, 1,878 and 1,853 cm^{-1} assigned to **Mn^{0}-dimer** (Supplementary Section 3.1 and Supplementary Table 5). This suggests that the promoted formation of **Mn^{I}-H** in the presence of **Fe-S** hinders the dimerization of the Mn(0) complex [$Mn^{0}(bpy)(CO)_3$] (**Mn^{0}-cat**) to **Mn^{0}-dimer**. In addition, the appearance of a set of ν_{CO} vibrations at 2,012, 1,935 and 1,920 cm^{-1} points to the formation of a neutral [$Mn(bpy)(CO)_3L$] (**Mn^{0}-L**) complex[29] (**L** being a neutral ligand, such as CH_3CN; Fig. 2d and Supplementary Fig. 15). Such a complex is not observed in the absence of **Fe-S** and we tentatively attribute its formation to a weak interaction between the reduced cluster $[Fe_4S_4(SPh)_4]^{3-}$ (**Fe-S^{-1}**) and **Mn^{I}-cat**, which triggers Br^{-} release and subsequent reduction of the cationic acetonitrile complex. In situ formation of HCOOH was further confirmed by the appearance of its characteristic vibration at 1,700 cm^{-1} (ref. [19]). When the potential of the IRSEC cell is shifted slightly further to the negative (to approximatively −1.85 V), we observed the initial fast increase of the vibrations associated with **Mn^{I}-H**, followed by a slow decay along with growth of the vibration at 1,700 cm^{-1}, suggesting intense HCOOH generation (Supplementary Fig. 17). The additional vibrations at 1,911 and 1,810 cm^{-1}, which grow further when the potential of the cell is shifted to more negative values, are attributed to $[Mn(bpy)(CO)_3]^{-}$ (**Mn^{-1}-cat**)[31]. **Mn^{-1}-cat** catalyses the selective reduction of CO_2 to CO and its gradual appearance at the most negative potentials is consistent with the increased FYs for CO observed in CPE experiments at potentials below −1.85 V.

Formation of **Mn^{I}-H** was further confirmed by the appearance of a hydride resonance at −3.12 ppm in the ^{1}H NMR spectrum of a 1:1 solution of **Mn^{I}-cat/Fe-S**, reduced by a CPE step at −1.65 V in CD_3CN followed by the addition of a CO_2 saturated TFE/CD_3CN solution (2 M, 30 µL) to the NMR tube (Fig. 2e, green spectrum). The simultaneous presence of a resonance at δ = 8.4 ppm, assigned to HCOOH, confirms the catalytic activity of the complex at that potential and explains the low intensity of the **Mn^{I}-H** signal, as it is consumed to generate HCOOH. Consequently, the appearance of the hydride resonance is more pronounced when the same experiment is carried out in the absence of CO_2 (Fig. 2e, blue spectrum). Using TFED instead of TFE in these experiments led to the disappearance of the **Mn^{I}-H** and HCOOH signals from the ^{1}H NMR spectra and the appearance of peaks at the same chemical shifts in the ^{2}H NMR spectrum (Supplementary Fig. 22). None of the signals associated with **Mn^{I}-H** were observed in the absence of **Fe-S** under identical conditions (Fig. 2e, yellow spectrum), with ^{1}H NMR confirming instead the formation of **Mn^{0}-dimer**, as observed in IRSEC experiments (Supplementary Section 4 and Supplementary Fig. 17). As suggested in the IRSEC experiments, ^{1}H NMR data confirmed that the formation of **Mn^{0}-dimer** on reduction is minimized in the presence of **Fe-S** (Supplementary Fig. 19), favouring instead the formation of a neutral **Mn^{0}-L** species. This **Mn^{0}-L** species appeared to be stable towards disproportionation at the experimental timescale (Supplementary Figs. 20 and 26).

Combined with CV measurements, the IRSEC and ^{1}H NMR data provide evidence for the formation of **Mn^{I}-H**. **Mn^{I}-H** generation is observed after the $1e^{-}$ reduction of **Mn^{I}-cat** to **Mn^{0}-cat**, which occurs at a potential at which **Fe-S** is already in the reduced **Fe-S^{-1}** state. CV and ^{1}H NMR data suggest that **Fe-S^{-1}** is oxidized on formation of **Mn^{I}-H**: the reversibility of the **Fe-S/Fe-S^{-1}** process is lost in the presence of TFE (Supplementary Fig. 6) and **Fe-S** appears in the ^{1}H NMR spectrum after addition of TFE to a 1:1 solution of **Mn^{I}-cat/Fe-S** reduced by a CPE step at −1.65 V (Supplementary Fig. 19). Nonetheless, thermodynamic and kinetic considerations rule out the possibility of an ET–PT mechanism mediated by **Fe-S** and generating **Mn^{I}-H** on protonation of **Mn^{-1}-cat**: the electrochemical generation of **Mn^{I}-H** via an ET–ET–PT pathway from **Mn^{I}-cat** occurs at −1.87 V in the presence of strong proton sources (such as morpholine in the presence of CO_2, $pK_a \approx 17$)[22]. This potential is more cathodic than that required for the generation of **Mn^{I}-H** in the presence of a CPET mediator occurring at −1.65 V. The absence of **Mn^{-1}-cat** features at this potential in ^{1}H NMR and IRSEC data in the absence of proton sources (Supplementary Figs. 14 and 19) confirms that **Mn^{-1}-cat** is not present in solution and that **Fe-S^{-1}** does not act as a redox mediator to promote its formation. This is in good agreement with the significantly more anodic potential of the **Fe-S/Fe-S^{-1}** couple with respect to all **Mn^{I}-cat** reduction processes. Most importantly, in the presence of weaker acids (for example, TFE in the presence of CO_2, pK_a = 25.1), we determined that CO_2 binding to **Mn^{-1}-cat**, generated on two successive ET steps, is kinetically much faster than proton binding (approximately 15 times faster; Supplementary Section 6 and Supplementary Fig. 27). These relative binding rates have been proposed to be the main reason for the high CO selectivity of **Mn^{I}-cat**, the formation of **Mn^{I}-H** being kinetically hindered in the presence of CO_2 (ref. [32]). The high selectivity for HCOOH observed here in the presence of **Fe-S** thus further confirms that the formation of the catalytically active Mn-H species does not result from a ET–PT pathway. In a related manner, the quantitative dimerization of **Mn^{0}-cat** observed in the absence of **Fe-S** at the potentials required for **Mn^{I}-H** formation (Supplementary Figs. 14 and 19) precludes a PT–ET mechanism. This is consistent with a CPET from an in situ-generated **[Fe-S]H** species to **Mn^{0}-cat** to generate **Mn^{I}-H**, in agreement with the kinetic isotope effect of 1.85 determined here and lying in the typical range observed for CPET steps (Supplementary Section 5). **Fe-S** acts here as a CPET mediator for the catalytic generation of a manganese hydride species. It highlights that the ability of Fe–S clusters to promote hydrogen atom transfer, which is known for stoichiometric reactions[21], can be exploited in a catalytic pathway.

Boundary conditions for CPET-mediated M-H generation

This prompted us to attempt to determine the thermodynamic and kinetic feasibility of such a CPET-mediated metal hydride generation.

a

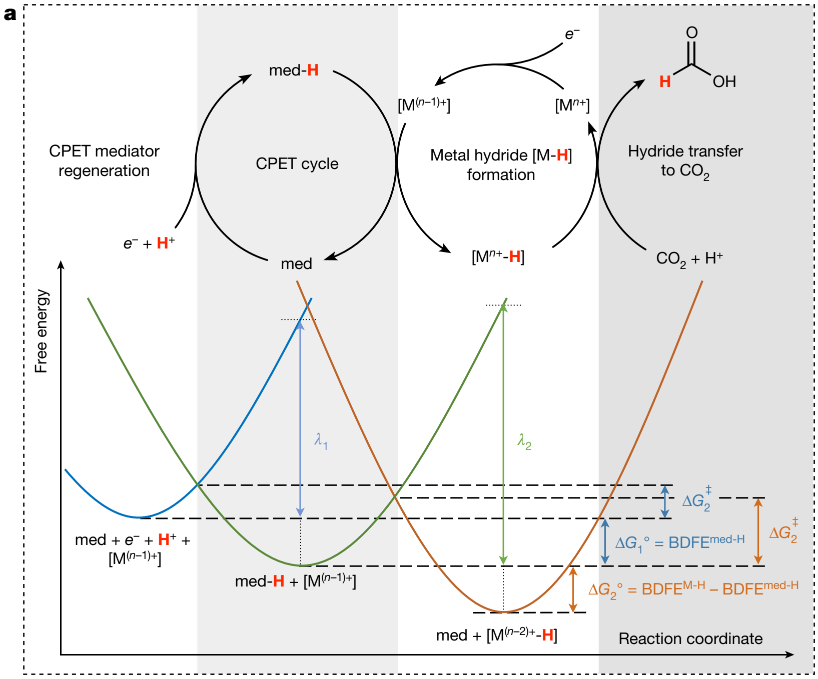

b

$$\Delta G^{\ddagger}_{\mathrm{CPET}} = \frac{(\Delta G^{\circ}_{\mathrm{CPET}} + \lambda)^2}{4\lambda} \quad (1)$$

$$k_{\mathrm{CPET}} = A \times \exp\left(\frac{-\Delta G^{\ddagger}_{\mathrm{CPET}}}{k_{\mathrm{B}}T}\right) = A \times \exp\left(\frac{-(\Delta G^{\circ}_{\mathrm{CPET}} + \lambda)^2}{4\lambda k_{\mathrm{B}}T}\right) \quad (2)$$

$$\mathrm{BDFE} = 1.346 \times \mathrm{p}K_{\mathrm{a}} + 23.06 \times E^{\circ} + C_{\mathrm{G}} \quad (3)$$

c

Boundary conditions for CPET-mediated M-H formation:

$\mathrm{BDFE}^{\mathrm{M\text{-}H}} > \mathrm{BDFE}^{\mathrm{med\text{-}H}}$

$\mathrm{p}K_{\mathrm{a}}^{\mathrm{H^{+}\text{-}donor}} < \mathrm{p}K_{\mathrm{a}}^{\mathrm{med\text{-}H}}$

Fig. 3 | Thermodynamic and kinetic considerations for catalytic CPET-mediated metal hydride formation. a, Schematic representation of the reaction steps in a CPET-mediated M-H generation followed by hydride transfer to CO_2 and the associated free-energy parabola representation. **b**, Equations (1) and (2) describe the free-energy barrier, $\Delta G^{\ddagger}_{\mathrm{CPET}}$, and the reaction rate constant, k_{CPET}, for a weakly coupled non-adiabatic CPET process; λ is the reorganization energy, A is the Arrhenius pre-exponential factor determined from overlap integrals of the electronic and proton vibrational states between the substrate and product, T is the absolute temperature and k_{B} is the Boltzmann constant. The Bordwell equation (3) enables estimating the BDFE values using K_{a} as the acidity constant of the protonated mediator med-H, E^0 as the reduction potential of the $\mathrm{med}^{0/-}$ couple, C_{G} being a solvent-dependent constant. **c**, Boundary conditions to be met to ensure catalytic CPET-mediated M-H generation.

Two CPET steps have to be considered: (1) the (re)generation of the med-H species with an electron and a proton; and (2) the overall transfer of an apparent hydrogen atom to the singly reduced metal site $[\mathrm{M}^{(n-1)+}]$ (Fig. 3a). Both steps can be interpreted in a Marcus-type formalism (Fig. 3b), in which a symmetric dependence between the rate of the reaction (k_{CPET}) and the thermodynamic driving force ($\Delta G^{\circ}_{\mathrm{CPET}}$) is expected, resulting in a lower activation barrier than required for the stepwise ET–PT and PT–ET processes. This dependence may be diminished by the fact that both a proton and an electron must synchronously tunnel, resulting in a potentially higher pre-exponential factor (A) than for isolated ET and PT steps. Nevertheless, the use of mild reducing agents and weak acid sources should mitigate that fact, and enable faster CPET rates, while being highly beneficial for catalytic purposes because the reaction proceeds at a lower overall driving force $\Delta G^{\circ}_{\mathrm{CPET}}$. Hence, considering the two steps of a catalytic, CPET-mediated generation of M-H species in the Marcus formalism, as presented in Fig. 3a, enables identification of the key parameters to optimize for an effective catalytic M-H formation that occurs at high rate and minimal thermodynamic cost while enabling regeneration of the CPET mediator.

First, efficient (re)generation of the CPET mediator requires minimizing the driving force ΔG°_{1} and the reorganization energy λ_1 for the generation step med → med-H. ΔG°_{1} corresponds to the BDFE of the med-H species, which can be estimated using the Bordwell equation (Fig. 3b). The two main parameters affecting the reorganization energy λ_1 are the solvent reorganization energy and the inner-sphere reorganization energy of the mediator, which is related to the intrinsic geometry change that occurs on generation of the med-H species. In the specific case of a CPET mechanism, the overall charge will not vary, and the main contributor to the overall reorganization energy will be the inner-sphere one. A good strategy to lower λ_1 is therefore to select a mediator with minimal structural and polarity changes on CPET.

Second, from a thermodynamic point of view, for the CPET to occur from med-H to the reduced metal complex M (that is, $\Delta G^{\circ}_{2} < 0$), the BDFE of the med-H species ($\mathrm{BDFE}^{\mathrm{med\text{-}H}}$) should be lower than the BDFE of the M-H species ($\mathrm{BDFE}^{\mathrm{M\text{-}H}}$) formed[33]. These values should, however, be close, to lower the associated kinetic energy barrier, as highlighted above.

Last, to ensure an efficient proton transfer from the proton source to the mediator, the relation $\mathrm{p}K_{\mathrm{a}}^{\mathrm{proton\ source}} \leq \mathrm{p}K_{\mathrm{a}}^{\mathrm{med\text{-}H}}$ should be fulfilled. Additional selection factors come into play when H_2 generation is not the reaction of interest and will be discussed below.

Hence, for the present system, an effective CPET can occur if $\mathrm{BDFE}^{\mathrm{[Fe\text{-}S]H}}$ is lower than $\mathrm{BDFE}^{\mathrm{Mn\text{-}H}}$. However, verifying this condition first implies determining these BDFEs, which were not previously reported. We determined $\mathrm{BDFE}^{\mathrm{[Fe\text{-}S]H}}$ here to be as low as 63.5 kcal mol^{-1}, in good agreement with the BDFE value of 60.5 kcal mol^{-1} recently reported for another Fe–S cluster bearing substituted thioaryloxide ligands[21]. The determination of this value necessitated evaluating the $\mathrm{p}K_{\mathrm{a}}$ value of **[Fe-S]H**, which we determined electrochemically using a protonated P1 phosphazene base (Supplementary Section 7) and found

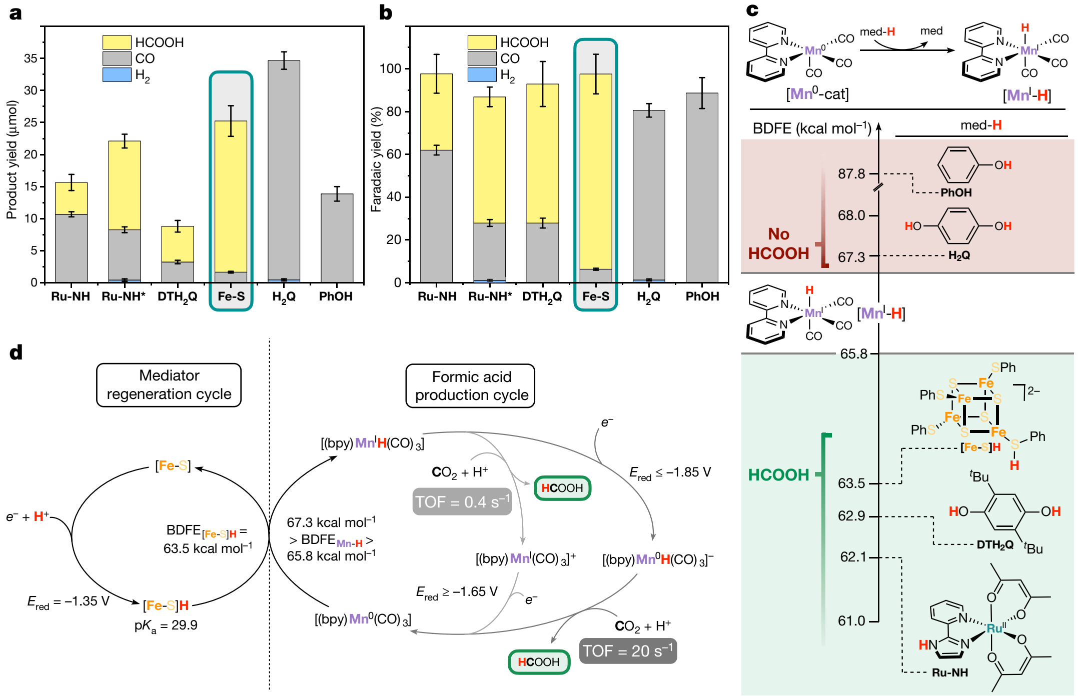

Fig. 4 | CO_2RR activity of Mn^I-cat in the presence of various CPET mediators. **a**,**b**, Product yields (**a**) and associated Faradaic yields (**b**) for CO_2RR using **Mn^I-cat** in the presence of various CPET mediators. The first three entries from the left correspond to experiments carried out in the presence of a proton source (0.2 M TFE, except for **Ru-NH*** where 1.5 M H_2O was used), whereas the other entries relate to catalytic tests carried out in the absence of a proton source and at high concentration of the CPET mediator (0.1–0.5 M), error bars indicate the systematic error of duplicate independent CPE measurements. **c**, Scaling relation of BDFE$^{\text{med-H}}$ with formic acid production, which led to the determination of BDFE$^{\text{Mn-H}}$ via the reaction shown at the top. The BDFE values mentioned here are summarized in Supplementary Section 6. **d**, Proposed mechanistic cycle for **Fe-S**-mediated **Mn^I-H** formation and subsequent transfer of the hydride to CO_2.

a value of 30.3 ± 0.3. This value lies in the expected range for this species assuming that a one-electron transfer increases the pK_a by 4–6 units compared to the oxidized species, as observed for synthetic Fe_2S_2 clusters[25]. The lower limit of BDFE$^{\text{Mn-H}}$ was estimated as 65.8 kcal mol^{-1} on the basis of CV and ^{1}H NMR data (Supplementary Section 8). This value is slightly higher than those reported for other manganese hydride complexes, such as $HMn(CO)_5$ (60 kcal mol^{-1}) and $HMn(CO)_4PPh_3$ (61 kcal mol^{-1})[22]. To further assess BDFE$^{\text{Mn-H}}$, we studied the CO_2 electroreduction activity and respective product ratios between CO and HCOOH of **Mn^I-cat** in the presence of a series of CPET mediators (Fig. 4a) covering a range of BDFE values around this estimated lower boundary. Figure 4b reveals that the amount of HCOOH is lowered with increasing the BDFE$^{\text{med-H}}$ of the CPET mediator using [Ru^{II}(acac)$_2$(PyImz)] (**Ru-NH**) (acac, acetylacetonate; PyImz, 2-pyridyl-imidazole) and 2,5-di-*tert*-butylhydroquinone (**DTH$_2$Q**) and vanished in the presence of 1,4-dihydroquinone (**H$_2$Q**) or phenol (**PhOH**), for which CO was observed to be the sole CO_2RR product (Supplementary Section 9). The presence of significant amounts of HCOOH as a reaction product reveals the formation of **Mn^I-H**, and enables bracketing BDFE$^{\text{Mn-H}}$ between 63.5 kcal mol^{-1} and 67.3 kcal mol^{-1}, in good agreement with the experimentally determined lower boundary of 65.8 kcal mol^{-1}. This first evaluation of BDFE$^{\text{Mn-H}}$ enables determination of the thermodynamic feasibility of the hydride transfer from **Mn^I-H** to CO_2 from a hydricity point of view[34,35]. The lower limit of hydricity of the **Mn^I-H** is estimated to be approximately 57.6 kcal mol^{-1} according to the standard reduction potential correlation (Supplementary Section 10). This is significantly higher than the thermodynamic threshold for HCOOH production (44 kcal mol^{-1})[35]. Such a hydride transfer to CO_2, occurring despite an apparently unfavourable driving force, was recently observed for a related Mn^I-H complex, and was proposed to be driven by the formation of a Mn^I-OCHO species[19]. To demonstrate that such a transfer could occur in the specific case of **Mn^I-H**, we reacted a solution of **Mn^I-H** prepared by CPE under CO_2, and observed the consumption of the **Mn^I-H** species and the appearance of [Mn^I(bpy)(CO)$_3$(OCHO)] (**Mn^I-OCHO**). (Supplementary Figs. 19 and 22). Nevertheless, the low rate observed for HCOOH generation when CPE is carried out at −1.65 V confirms that **Mn^I-H** needs to be further reduced to generate a more active catalyst. This reduction occurs at approximately −1.85 V to generate a formal Mn(0)-hydride species (**Mn^0-H**), whose BDFE value can be approximated as 10–15 kcal mol^{-1} lower than that of **Mn^I-H**[36,37]. The hydricity value of **Mn^0-H** lies in the range observed for very selective CO_2RR to HCOOH catalysts[34,35], and is hence fully consistent with the observed high selectivity and rate for HCOOH production observed here. This latter finding permits us to validate the reaction pathway for the fast electrocatalytic CO_2RR to HCOOH by the composite system (**Mn^I-cat/Fe-S**) shown in Fig. 4d; **Fe-S** mediates a CPET step to electrogenerated **Mn^0-cat** affording **Mn^I-H** while hindering the competitive dimerization of **Mn^0-cat**; **Mn^I-H** is further reduced to generate **Mn^0-H**, which subsequently mediates a hydride transfer to CO_2 to produce HCOOH. The reduction to **Mn^0-H** remains thermodynamically more favourable (approximately 65 mV difference in peak potential) than the direct generation of **Mn^I-H** in the absence of a CPET mediator via the protonation of **Mn^{-1}-cat** (Supplementary Fig. 6).

The determined BDFE and hydricity values also shine a light on the observed selectivity towards HCOOH generation when **Mn^I-cat** is used in photochemical CO_2RR. The typical decrease of the BDFE for the composite system made of the photosensitizer and proton source, to values below 40 kcal mol^{-1} on light excitation[38], is sufficient to trigger the formation of **Mn^I-H** and HCOOH production. Similarly, this work may provide a rationale for the recently observed change of CO_2RR selectivity to HCOOH of **Mn^I-cat** in the presence of an isopropanol/triethylamine mixture, which was published during the reviewing of the present work[39]. The interaction between isopropanol and triethylamine in the presence of CO_2 results in a lowering of the pK_a of over 20 units, which could explain lowering of the effective BDFE value of isopropanol below 65.8 kcal mol^{-1} and the generation of **Mn^I-H** by CPET.

In addition, these electrocatalytic tests in the presence of various CPET mediators highlight several key features regarding their role in the catalytic activity of **Mn^I-cat**. First, a substantial enhancement of CO_2RR activity of **Mn^I-cat** was also observed in the presence of CPET mediators such as **H_2Q** without change of selectivity (Figs. 2b and 4a), promoting the selective CO_2RR to CO. We assigned this strong rate enhancement to the fact that the BDFE value of **H_2Q** is too high to enable generation of **Mn^I-H** species, but that **H_2Q** still acts as a CPET mediator to enhance the CO_2RR rate, promoting faster proton–electron transfer to the activated CO_2 molecule in the known CO_2 to CO reaction pathway using **Mn^I-cat**[32]. Such rate enhancement without a change in selectivity has recently been reported for CO_2RR to CO using iron porphyrin complexes in combination with a synthetic NADH analogue as the CPET mediator[40]. Second, the catalytic CO_2RR performances for HCOOH obtained using **Fe-S** as the mediator ($TON_{HCOOH} \approx 4$) are significantly better than using **Ru-NH** ($TON_{HCOOH} \approx 0.8$) and **DTH_2Q** ($TON_{HCOOH} \approx 0.9$) (Supplementary Table 1).

The small difference in BDFE values of the above-mentioned CPET mediators (below 1 kcal mol^{-1} between **Ru-NH**, **DTH_2Q** and **Fe-S**) is unlikely to explain this strong discrepancy in CO_2RR TONs for HCOOH. The regeneration step was analysed in detail (Supplementary Section 2.5), and it was found that the lower TONs resulted from the two points identified above as critical for an efficient regeneration of the CPET mediators, namely, the ability of the proton source to transfer a proton to the mediator and the fast reduction of the oxidized mediator. These observations enable headlining a key criterion to consider for the rational choice of a CPET mediator for catalytic M-H generation according to Fig. 3a, when H_2 production must be avoided. Once the optimal BDFE value of the CPET mediator for a targeted M-H$^{(n-1)+}$ formation has been determined according to the boundary conditions listed in Fig. 3c, the Bordwell equation sets the relationship between the E^0 and pK_a to be verified for the CPET mediator. The optimal mediator should be chosen to have the highest possible pK_a value, to enable efficient regeneration of the mediator in the presence of weak acids while disfavouring the protonation of the hydride species affording H_2. This imposes the requirement that the optimal E^0 value of the CPET mediator should be as cathodic as possible while remaining in the potential window of interest for the system, and being determined by either the potential for the direct 2e^- reduction of the complex of interest or the solvent/substrate wall.

Conclusions

The results presented here further highlight that **Fe-S** is a remarkably effective CPET mediator for the current catalytic system, as it perfectly fulfils the boundary conditions described in Fig. 3c, and the close BDFE values of **[Fe-S]H** and **Mn^I-H**, together with the intrinsic low reorganization energy of **Fe-S**, enable maximizing the efficiency of the (re)generation of the CPET mediator. Related to this, the efficient regeneration in the presence of mild proton sources prevents direct protonation of the **Mn-H** generated on CPET and ensures high selectivity against undesired H_2 evolution.

These results serve as a proof of concept for the rational choice of a CPET mediator enabling catalytic metal hydride formation, and showcase the potential of synthetic Fe–S clusters as CPET mediators owing to their low reorganization energy and the simple tuning of their redox potential on modulation of the ligand framework. A wide range of catalytic reactions involving M-H could benefit from the approach and guiding principles presented here.

Online content

Any methods, additional references, Nature Research reporting summaries, source data, extended data, supplementary information, acknowledgements, peer review information; details of author contributions and competing interests; and statements of data and code availability are available at https://doi.org/10.1038/s41586-022-04874-z.

1. Bullock, R. M. & Helm, M. L. Molecular electrocatalysts for oxidation of hydrogen using Earth-abundant metals: shoving protons around with proton relays. *Acc. Chem. Res.* **48**, 2017–2026 (2015).
2. Francke, R., Schille, B. & Roemelt, M. Homogeneously catalyzed electroreduction of carbon dioxide—methods, mechanisms, and catalysts. *Chem. Rev.* **118**, 4631–4701 (2018).
3. Nitopi, S. et al. Progress and perspectives of electrochemical CO_2 reduction on copper in aqueous electrolyte. *Chem. Rev.* **119**, 7610–7672 (2019).
4. Elgrishi, N., Kurtz, D. A. & Dempsey, J. L. Reaction parameters influencing cobalt hydride formation kinetics: implications for benchmarking H_2-evolution catalysts. *J. Am. Chem. Soc.* **139**, 239–244 (2017).
5. Huang, T., Rountree, E. S., Traywick, A. P., Bayoumi, M. & Dempsey, J. L. Switching between stepwise and concerted proton-coupled electron transfer pathways in tungsten hydride activation. *J. Am. Chem. Soc.* **140**, 14655–14669 (2018).
6. Kurtz, D. A. et al. Redox-induced structural reorganization dictates kinetics of cobalt(III) hydride formation via proton-coupled electron transfer. *J. Am. Chem. Soc.* **143**, 3393–3406 (2021).
7. Noh, H. et al. Redox-mediator-assisted electrocatalytic hydrogen evolution from water by a molybdenum sulfide-functionalized metal–organic framework. *ACS Catal.* **8**, 9848–9858 (2018).
8. Rausch, B., Symes, M. D. & Cronin, L. A bio-inspired, small molecule electron-coupled-proton buffer for decoupling the half-reactions of electrolytic water splitting. *J. Am. Chem. Soc.* **135**, 13656–13659 (2013).
9. Dutta, A., Appel, A. M. & Shaw, W. J. Designing electrochemically reversible H_2 oxidation and production catalysts. *Nat. Rev. Chem.* **2**, 244–252 (2018).
10. Smith, N. E., Bernskoetter, W. H. & Hazari, N. The role of proton shuttles in the reversible activation of hydrogen via metal–ligand cooperation. *J. Am. Chem. Soc.* **141**, 17350–17360 (2019).
11. Badalyan, A. & Stahl, S. S. Cooperative electrocatalytic alcohol oxidation with electron-proton-transfer mediators. *Nature* **535**, 406–410 (2016).
12. McLoughlin, E. A., Armstrong, K. C. & Waymouth, R. M. Electrochemically regenerable hydrogen atom acceptors: mediators in electrocatalytic alcohol oxidation reactions. *ACS Catal.* **10**, 11654–11662 (2020).
13. Galvin, C. M. & Waymouth, R. M. Electron-rich phenoxyl mediators improve thermodynamic performance of electrocatalytic alcohol oxidation with an iridium pincer complex. *J. Am. Chem. Soc.* **142**, 19368–19378 (2020).
14. Chalkley, M. J., Garrido-Barros, P. & Peters, J. C. A molecular mediator for reductive concerted proton–electron transfers via electrocatalysis. *Science* **369**, 850–854 (2020).
15. Anson, C. W. & Stahl, S. S. Cooperative electrocatalytic O_2 reduction involving Co(salophen) with *p*-hydroquinone as an electron–proton transfer mediator. *J. Am. Chem. Soc.* **139**, 18472–18475 (2017).
16. Bourrez, M., Molton, F., Chardon-Noblat, S. & Deronzier, A. [Mn(bipyridyl)$(CO)_3$Br]: an abundant metal carbonyl complex as efficient electrocatalyst for CO_2 reduction. *Angew. Chem. Int. Ed. Engl.* **50**, 9903–9906 (2011).
17. Takeda, H., Koizumi, H., Okamoto, K. & Ishitani, O. Photocatalytic CO_2 reduction using a Mn complex as a catalyst. *Chem. Commun.* **50**, 1491–1493 (2014).
18. Wang, X. et al. Site-isolated manganese carbonyl on bipyridine-functionalities of periodic mesoporous organosilicas: efficient CO_2 photoreduction and detection of key reaction intermediates. *Chem. Sci.* **8**, 8204–8213 (2017).
19. Rønne, M. H. et al. Ligand-controlled product selectivity in electrochemical carbon dioxide reduction using manganese bipyridine catalysts. *J. Am. Chem. Soc.* **142**, 4265–4275 (2020).
20. Bhattacharya, M., Sebghati, S., VanderLinden, R. T. & Saouma, C. T. Toward combined carbon capture and recycling: addition of an amine alters product selectivity from CO to formic acid in manganese catalyzed reduction of CO_2. *J. Am. Chem. Soc.* **142**, 17589–17597 (2020).
21. Saouma, C. T., Morris, W. D., Darcy, J. W. & Mayer, J. M. Protonation and proton-coupled electron transfer at S-ligated [4Fe-4S] clusters. *Chem. Eur. J.* **21**, 9256–9260 (2015).
22. Tilset, M. & Parker, V. D. Solution homolytic bond dissociation energies of organotransition-metal hydrides. *J. Am. Chem. Soc.* **111**, 6711–6717 (1989).
23. Senger, M. et al. Proton-coupled reduction of the catalytic [4Fe-4S] cluster in [FeFe]-hydrogenases. *Angew. Chem. Int. Ed. Engl.* **56**, 16503–16506 (2017).
24. Camba, R. et al. Mechanisms of redox-coupled proton transfer in proteins: role of the proximal proline in reactions of the [3Fe-4S] cluster in *Azotobacter vinelandii* ferredoxin I. *Biochemistry* **42**, 10589–10599 (2003).
25. Albers, A. et al. Fast proton-coupled electron transfer observed for a high-fidelity structural and functional [2Fe–2S] Rieske model. *J. Am. Chem. Soc.* **136**, 3946–3954 (2014).
26. Kennepohl, P. & Solomon, E. I. Electronic structure contributions to electron-transfer reactivity in iron–sulfur active sites: 3. Kinetics of electron transfer. *Inorg. Chem.* **42**, 696–708 (2003).

27. Sigfridsson, E., Olsson, M. H. M. & Ryde, U. Inner-sphere reorganization energy of iron–sulfur clusters studied with theoretical methods. *Inorg. Chem.* **40**, 2509–2519 (2001).
28. Jordan, R. F. & Norton, J. R. in *Mechanistic Aspects of Inorganic Reactions* (eds Rorabacher, D. B. & Endicott, J. F.) ACS Symposium Series Vol. 198, Ch. 17, 403–423 (American Chemical Society, 1982).
29. Franco, F. et al. Local proton source in electrocatalytic CO_2 reduction with [Mn(bpy–R)$(CO)_3$Br] complexes. *Chem. Eur. J.* **23**, 4782–4793 (2017).
30. Cotton, F. A., Down, J. L. & Wilkinson, G. Infrared spectra of manganese carbonyl hydride and deuteride. *J. Chem. Soc.* 833–837 (1959).
31. Machan, C. W., Sampson, M. D., Chabolla, S. A., Dang, T. & Kubiak, C. P. Developing a mechanistic understanding of molecular electrocatalysts for CO_2 reduction using infrared spectroelectrochemistry. *Organometallics* **33**, 4550–4559 (2014).
32. Riplinger, C., Sampson, M. D., Ritzmann, A. M., Kubiak, C. P. & Carter, E. A. Mechanistic contrasts between manganese and rhenium bipyridine electrocatalysts for the reduction of carbon dioxide. *J. Am. Chem. Soc.* **136**, 16285–16298 (2014).
33. Mayer, J. M. Understanding hydrogen atom transfer: from bond strengths to Marcus theory. *Acc. Chem. Res.* **44**, 36–46 (2011).
34. Waldie, K. M., Ostericher, A. L., Reineke, M. H., Sasayama, A. F. & Kubiak, C. P. Hydricity of transition-metal hydrides: thermodynamic considerations for CO_2 reduction. *ACS Catal.* **8**, 1313–1324 (2018).
35. Ceballos, B. M. & Yang, J. Y. Directing the reactivity of metal hydrides for selective CO_2 reduction. *Proc. Natl Acad. Sci. USA* **115**, 12686–12691 (2018).
36. Parsell, T. H., Yang, M.-Y. & Borovik, A. S. C–H Bond cleavage with reductants: re-investigating the reactivity of monomeric $Mn^{III/IV}$–oxo complexes and the role of oxo ligand basicity. *J. Am. Chem. Soc.* **131**, 2762–2763 (2009).
37. Pattanayak, S. et al. Spectroscopic and reactivity comparisons of a pair of bTAML complexes with $Fe^{V}{=}O$ and $Fe^{IV}{=}O$ units. *Inorg. Chem.* **56**, 6352–6361 (2017).
38. Qiu, G. & Knowles, R. R. Rate–driving force relationships in the multisite proton-coupled electron transfer activation of ketones. *J. Am. Chem. Soc.* **141**, 2721–2730 (2019).
39. Madsen, M. R. et al. Promoting selective generation of formic acid from CO_2 using Mn(bpy)$(CO)_3$Br as electrocatalyst and triethylamine/isopropanol as additives. *J. Am. Chem. Soc.* **143**, 20491–20500 (2021).
40. Smith, P. T., Weng, S. & Chang, C. J. An NADH-inspired redox mediator strategy to promote second-sphere electron and proton transfer for cooperative electrochemical CO_2 reduction catalyzed by iron porphyrin. *Inorg. Chem.* **59**, 9270–9278 (2020).

Data availability

The data that support the findings of this study (catalytic activity tests, cyclic voltammograms, NMR, UV–Vis and IRSEC spectra) are available within the paper and its Supplementary Information files.

Acknowledgements We thank L. Grunwald and A. Mouchfiq for technical assistance and preliminary studies, and R. Verel for assistance with NMR studies. We acknowledge funding from Agence Nationale pour la Recherche, ANR Jeune Chercheur-Jeune Chercheuse ANR-17-CE05-0021 (S.D., V.M.); European Research Council (ERC) under the European Union's Horizon 2020 research and innovation programme (grant agreement no. 853064 (S.D., F.M., V.M.)); and Swiss National Science Foundation (SNSF) project funding (grant no. 200021_197153 / 1 (V.M.)).

Author contributions S.D. and V.M. conceptualized the study and were responsible for the methodology. S.D., F.M. and E.B. undertook the investigations. V.M. was responsible for funding acquisition and supervision. M.F. and V.M. administered the project. S.D., F.M. and V.M. wrote the original draft. All authors reviewed and edited the manuscript.

Competing interests The authors declare no competing interests.

Additional information
Supplementary information The online version contains supplementary material available at https://doi.org/10.1038/s41586-022-04874-z.
Correspondence and requests for materials should be addressed to Victor Mougel.
Peer review information *Nature* thanks the anonymous reviewers for their contribution to the peer review of this work.